Optics Letters

Optical center of a luminescent solar concentrator

JINGJIAN ZHOU,[1,*] JING HUANG,[1,2,3] AND ILYA SYCHUGOV[1,4]

[1]Department of Applied Physics, KTH - Royal Institute of Technology, Stockholm 11419, Sweden
[2]School of Environmental and Biological Engineering, Nanjing University of Science and Technology, Nanjing 210094, China
[3]e-mail: jinghuang@njust.edu.cn
[4]e-mail: ilyas@kth.se
*Corresponding author: jingjian@kth.se

Received 16 June 2022; revised 22 August 2022; accepted 28 August 2022; posted 30 August 2022; published 21 September 2022

This Letter introduces a novel, to the best of our knowledge, approach to estimate the power conversion efficiency (PCE) of a square luminescent solar concentrator (LSC) by point excitations on the "optical centers." Predicted by theoretical calculations, photoluminescence emissions from these optical centers experience almost the same average optical path as those from the whole device under uniform illumination. This is experimentally verified by a 20×20 cm^2 silicon quantum dot-based LSC, with a negligible error between the predicted PCE and the measured one. This method provides a convenient way to estimate the photovoltaic performance of large-area LSC devices with basic laboratory instruments.

https://doi.org/10.1364/OL.467917

A planar waveguide with uniformly embedded light sources is a generic concept used in laser phosphor displays [1], solar-pumped lasers [2], and luminescent solar concentrators (LSCs). The latter were first proposed in the early 1970s [3], with the main purpose to concentrate sunlight by means of photoluminescence (PL). The fluorophores embedded in the host matrices absorb a part of sunlight and re-emit light. A significant fraction of PL emission (~75% for a slab with a refractive index of 1.5) is trapped in the waveguide by total internal reflection until it reaches the edges for conversion to electricity. In recent years, LSCs have gained much attention as semitransparent building-integrated photovoltaic (BIPV) units balancing PV performance and aesthetic quality, commonly known as "solar windows" [4].

The active light-converting materials are typically organic dyes [5], semiconductor quantum dots [4], rare-earth ions [6], or metal nanoclusters [7]. For efficient operation, a high photoluminescence quantum yield (PLQY) and a large Stokes shift are required to reduce reabsorption loss of the emitted light. The typical matrices are glass or polymers such as poly-(methylmethacrylate) (PMMA) and off-stoichiometry thiol-ene (OSTE) [8]. A triplex laminate structure is also used [8], with a thin polymer interlayer sandwiched in between two glass pieces. The fluorophores should also be well dispersible inside, translating to low scattering and haze for better energy conversion efficiency and glazing function.

Over the years, efforts have been devoted to improving the power conversion efficiency (PCE) of LSCs [9]. In addition, extending the device size to large areas ($\geq$100 cm^2) becomes significant for practical applications. For the LSC PV performance characterization, following the conventional method requires a correspondingly large solar simulator. This approach, however, is not feasible when it comes to truly large LSCs (tens of cm) for in-the-lab device measurements. Recently, regional measurements were introduced to analyze the PV performance and the spectral response of large-area LSCs with a shifting mask and a piece of solar cell placed at different edge regions [10,11]. However, scanning numerous excitation points all over the large-area device may not always be practical either.

In this Letter, a new approach for estimating the PV performance of large-area LSCs from point excitations is introduced. These points are named as "optical centers" of an LSC in analogy with the center of mass in mechanics. It is defined as points from which the average optical path to the device edges is equal to that of the whole device under uniform excitation. Here, the response to point excitations for a planar waveguide is analytically derived, and the position of such optical centers is found to be at ~82% of the center-edge distance for the square geometry. Using selective excitation to this spot, the short-circuit current I_{sc} of the whole device can be obtained by linearly scaling with the excitation area. This hypothesis was then successfully verified by a set of measurements on a 20×20 cm^2 LSC with silicon quantum dots (Si QDs) as fluorophores. It is shown that using the average I_{sc} measured at the optical center, the PCE of this device can be very well predicted within a measurement error, confirming that this approach is practically useful for the experimental evaluation of the PV performance of large-area LSCs.

In this work, we consider square geometry, which is very common for LSCs. Previously, we found that uniform excitation square and circular geometries were very similar in terms of optical path distribution from an isotropic emitter [12]. Using this established similarity here, we can derive simple expressions for the average optical path for a point excitation.

Consider a square with side length $2a$ and a circle of the same area with radius R. These two quantities are related by $R = 2a/\sqrt{\pi} \approx 1.128a$. First, we derive an analytical formula for the average optical path inside a circle for an emitter placed at a distance ρ from its center in 2D [Fig. 1(a), inset]. An optical ray emitted at an angle θ from the radial direction will experience path r until reaching the perimeter, where it is absorbed (all edges covered with solar cells). These two quantities are related

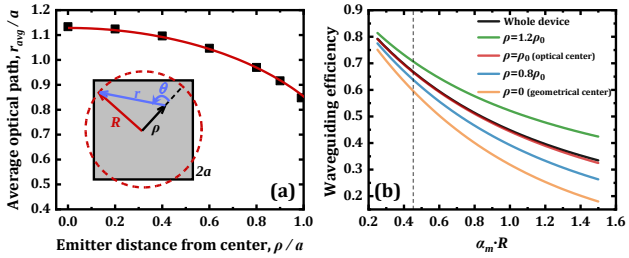

Fig. 1. (a) Average optical path as a function of the point excitation position. Square dots represent numerical simulation values for a square, while the line is for a circle of the same area from Eq. (3). Inset is a schematic illustration. (b) Waveguiding efficiencies for point (green, red, blue, orange solid lines) and uniform (black solid line) excitations of an LSC as a function of the dimensionless variable $\alpha_m R$. The vertical gray dashed line indicates the LSC device used in this work for the experimental validation.

as

$$\theta = \arccos\left(\frac{R^2 - \rho^2 - r^2}{2\rho r}\right). \tag{1}$$

The emitter is isotropic, so the angular distribution of its intensity $dI/d\theta$ is a constant. Then one can express emitted intensity distribution over the optical paths as

$$p(r) = \frac{dI}{dr} = \frac{dI}{d\theta}\frac{d\theta}{dr} = \frac{R^2 - \rho^2 + r^2}{\pi r\sqrt{-\rho^4 + 2(R^2 + r^2)\rho^2 - (R^2 - r^2)^2}}, \tag{2}$$

where the constant was chosen to satisfy the normalization condition $\int_{R-\rho}^{R+\rho} p(r)dr = 1$, so that $p(r)$ has the meaning of a probability density function.

Then the average optical path is a first moment of this distribution. Integration yields

$$r_{avg}(\rho*) = \frac{(1+\rho*)\cdot E(\gamma) + (1-\rho*)\cdot K(\gamma)}{\pi} R, \tag{3}$$

where $\rho*$ is the dimensionless distance from the center ($\rho* = \rho/R$), $\gamma = 2\sqrt{\rho*}/(1+\rho*)$, and $K(\gamma), E(\gamma)$ are complete elliptic integrals of the first and second kind, respectively. It is shown as a function of ρ/a in Fig. 1(a) as a red line. It is seen that the average optical path shortens when the emitter approaches the absorbing perimeter, as would be expected.

To validate the applicability of this formula for a square geometry, we plotted numerically calculated average optical paths for an isotropic emitter placed at several points inside the same area square (details in the Supplementary material). Those are shown as square dots in the same units in Fig. 1(a), confirming similarity of these two geometries in this sense. So the first conclusion of this analysis is that the position of a point excitation in 2D geometry (x,y) for a square waveguide can be effectively reduced to the function of a single variable ρ.

Next, we postulate that there is a spot on the LSC (at a distance from the center ρ_0), where the average optical path for an isotropic emitter equals to that of the whole device under uniform illumination. The latter was derived in [12] for a circle as $8R/3\pi$, therefore,

$$r_{avg}(\rho_0*) = \frac{8}{3\pi} R. \tag{4}$$

The numerical solution of this equation can be found using Eq. (3). In the units of length, it is $\rho_0 = 0.731R$. For a square with the side length $2a$, this is equivalent to

$$\rho_0 = 0.824a. \tag{5}$$

We assign these points to the optical centers of a square planar waveguide.

In general, however, the average optical path may not necessarily represent a valid parameter for light propagation assessment. For example, because the distribution of Eq. (2) is bimodal, the presence of attenuation may result in substantially different waveguiding efficiencies than those predicted using r_{avg}. Another necessary realistic aspect to consider is the 3D geometry of such planar waveguides.

Due to the total internal reflection, all photons emitted outside the escape cone (42° for a glass or plastic slab) will be waveguided to the device edge. The distribution of optical paths for such photons is therefore quite narrow and an average value for the out-of-plane emission can be used [13]. It was previously shown that all 2D optical paths can be simply extended by a factor $k \approx 1.144$ [12]. Changing variables ($l = kr$) from $p(r)$, the normalized probability density function $q(l)$ for the 3D case becomes

$$q(l) = \frac{p(l/k)}{k}. \tag{6}$$

Using this formula, we can compare the waveguiding efficiency for the single spot excitation with the total area illumination case in the presence of attenuation. Let the attenuation coefficient be α [cm^{-1}], which in practice can represent a matrix absorption coefficient ($\alpha \approx \alpha_m$) when only considering the matrix absorption loss. Then the waveguiding efficiency for a spot excitation at position ρ is

$$f_{sp} = \int_{l\min}^{l\max} \exp(-\alpha_m L) q(l) dl, \tag{7}$$

where $l_{\min} = k(R-\rho)$ and $l_{\max} = k(R+\rho)$. This function is shown for four different values of ρ (0, $0.8\rho_0$, ρ_0, $1.2\rho_0$) in Fig. 1(b). Dimensionless variable $\alpha_m R$ is limited by the upper LSC critical size ($\alpha_m R$<1.5), as introduced in [12]. However, the expression for the waveguiding efficiency under uniform illumination was previously derived [12]:

$$f_{LSC} = -\frac{M_1(2\alpha_m R k)}{\alpha_m R k}, \tag{8}$$

where M_1 is a modified Struve function of the second kind. The f_{LSC} function is shown in Fig. 1(b) as a black line. The waveguiding efficiencies are shown to be nearly identical for point excitation to the optical center and for uniform excitation in the considered range (red and black lines). Thus, the concept of the LSC optical center is theoretically validated under realistic conditions of attenuation and 3D geometry. Note that for fluorophores with non-negligible reabsorption coefficients α_{re}, this concept should still be applicable as long as the matrix absorption is the main loss mechanism ($\alpha_m > \alpha_{re}$). In addition, for a certain device (given $\alpha_m R$), the further the excitation point is from the center will mean a higher waveguiding efficiency. Moreover, a larger device (larger $\alpha_m R$) will result in a larger waveguiding efficiency gap between the geometrical center and the optical center (or whole device). In practice, it implies that the photocurrent difference between exciting geometrical and optical centers becomes quite substantial for large-area devices. Consequently, it is reasonable to deduce the I_{sc} value of the whole device from that of the optical center measurement.

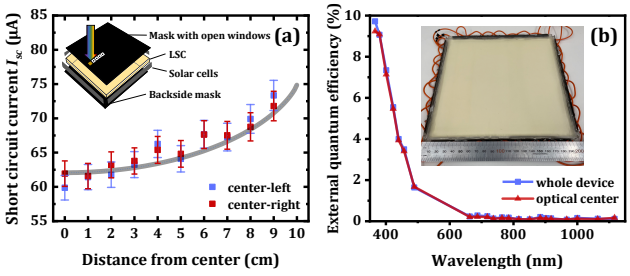

Fig. 2. (a) Short-circuit current under point excitations along two directions (center-left in blue and center-right in red) of a $20 \times 20\,\mathrm{cm}^2$ LSC under 0.9 AM1.5G. The gray solid line indicates the predicted trend. Note that due to the fabrication procedure of layered polymerization, only the directions non-crossing interfacial optical defects were considered. (b) External quantum efficiency under the optical center illumination (red) and uniform illumination of the whole device (blue). Inset is a photograph of the $20 \times 20\,\mathrm{cm}^2$ device.

To verify our hypothesis, a $20 \times 20\,\mathrm{cm}^2$ ($a = 10\,\mathrm{cm}$, $R \approx 11.3$ cm) low-haze LSC device based on luminescent Si QDs was used for the experimental validation. The device fabrication procedure can be found elsewhere [14]. In the triplex laminate structure, an off-stoichiometry thiol-ene (OSTE) polymer interlayer is of 3-mm thickness, and glass sheets are of 2-mm thickness each. Altogether ~60 mg of near-infrared-emitting (PL peak position ~870 nm, PLQY ~50%) Si QDs are uniformly dispersed in the polymer interlayer. The transmittance, absorption, reflectance, and haze spectra of this device are shown in Fig. S1 (Supplement 1). Note that this device is highly transparent (visible light transparency of ~90%) and thus not optimized for high power generation. Under the standard AM1.5G, ~8.3% of solar power is absorbed for the ensuing conversion to electricity (Fig. S2, Supplement 1). As reported previously [12], the matrix absorption coefficient α_m is $0.04\,\mathrm{cm}^{-1}$ for OSTE and of similar value for the low-iron glass applied here. Therefore, the dimensionless variable for this device is $\alpha_m R \approx 0.45$ [marked as a dashed line in Fig. 1(b)]. Details of the attached solar cells and the solar simulator used for the test can be found in Supplement 1l.

For excitation position-dependent measurements, two directions (center-left and center-right) of the LSC were probed under a series of point excitations by shifting the $1 \times 1\,\mathrm{cm}^2$ opening positions on the mask (details in Supplement 1). As shown in Fig. 2(a), a clear rising trend of I_{sc} from the center to the edge along both directions was observed. An analytical curve [gray curve in Fig. 2(a)] can be drawn by considering the matrix absorption loss for the average optical path r_{avg} under different point excitation positions [Fig. 1(a)] and the linearity of the short-circuit current with irradiance as $I_{sc}(\rho) = I_0 e^{-\alpha_m k r_{avg}(\rho)}$. As can be seen, the experimental data match well with the predicted trend with proportionality coefficient I_0 being the only fitting parameter.

To independently verify that the observed trend indeed originates from the luminescence waveguiding and not from random stray light or direct light on solar cells, we performed external quantum efficiency (EQE) measurements under the optical center (8 cm from the geometrical center) and whole device illumination. For the LSC device, EQE(λ) is the ratio of generated electrons by the edge solar cells to incident photons on the device top area. To block the direct illumination of solar cells, four "roofs" (each 5 mm wide) were applied at the top of the device edges in the case of the whole device illumination (in the case of point excitation, those are redundant thanks to the mask). As shown in Fig. 2(b), the EQE curves are consistent with the shape of the absorption spectrum of Si QDs (Fig. S1, Supplement 1). More importantly, both EQE curves are essentially identical, indicating almost the same short-circuit current density ($\mathrm{mA/cm}^2$) after being integrated with the solar spectrum. Moreover, the EQEs are close to zero above 650 nm, implying almost no contribution from the direct illumination or stray light, validating previous results.

Verification of the signal origin being from QD PL is essential for correct evaluation and application of the optical center method. Another aspect to consider is the size of the solar cell modules, as discussed in detail in Supplement 1. Briefly, to correctly resolve optical path variations under the point excitation, small size solar cells units, connected in parallel, are necessary. Otherwise, the I_{sc} of a solar cell will be limited by the lowest I_{sc} among the in-series connected p-n junctions (longest optical path). An example is shown in Figs. S3 and S4 in Supplement 1, where four-fold longer solar cells units were attached to the device edges. In that case, the trend, which is clearly visible in Fig. 2(a), becomes disrupted when approaching the edges.

After the optical center concept has been experimentally verified, we are in the position to discuss practical implementations. The most straightforward application is the short-circuit current evaluation of the whole device from the optical center excitation. To minimize the impact from the solar simulator non-uniformity, each I_{sc_oc} value under the optical center excitation was measured at each orthogonal direction under the solar simulator by spinning both the device and the mask, yielding an average I_{sc_oc} value of ~79 μA (±3 μA) under standard AM1.5G. Multiplying by the opening area ratio (400:1), one can predict I_{sc} under uniform illumination to be ~31.6 mA (±1.2 mA), which is very close to the measured value of ~33 mA (±0.5 mA) by the conventional method, matching within measurement error (I-V curve shown in Fig. S5, left, Supplement 1). We attribute this small error to the measurements instead of the mathematical assumptions, most likely due to the slight non-uniformity of the irradiance from the solar simulator and the LSC device. This confirms the plausibility of single excitation spot measurements for the whole device evaluation in terms of photocurrents.

Next, we can extend the method of predictive ability to the power conversion efficiency (PCE), which is an important figure of merit for photovoltaic devices. To accomplish that, the open circuit voltage and the fill factor (FF) need to be estimated in addition to the short-circuit current. However, under optical center excitations, the V_{oc} is limited by the lowest V_{oc} among the solar cells connected in parallel (farthest solar cells from the open window), and we instead suggest two methods for the estimation of V_{oc} and FF.

On average, for each piece of solar cell, ~1 mA (32 pieces in parallel) of current can be coarsely estimated. This estimation does not introduce a large error since the open circuit voltage grows logarithmically to the incident irradiance (or to the short-circuit current, which is linear to irradiance) [15].

By tuning the irradiance under the solar simulator (either percentage of AM1.5G or monochromatic light), the I-V curve (Fig. S5, right, Supplement 1) of a single piece of solar cell was recorded to simulate device operation conditions delivering

I_{sc_s} of ~1 mA. Then the open circuit voltage was ~2.01 V and the fill factor was ~0.63, which are indeed almost the same as measured ones for the operating LSC (Fig. S5, left, Supplement 1). Alternatively, considering the known logarithmic relationship between the V_{oc} of the solar cell and the incident irradiance similar values can be obtained, as detailed in the Supporting Information.

At last, the procedure of whole device PCE estimates from point excitation measurements can be summarized. (i) Measure the average I_{sc_oc} with only the window at the optical center open. Scaling with the whole device area gives the overall I_{sc} under uniform illumination. (ii) Consider the solar cell connections and estimate the I_{sc_s} value for a single piece of solar cell. Place a single piece of solar cell under the solar simulator, and tune the irradiance until the solar cell delivers the same I_{sc_s}. (iii) Extract the open circuit voltage V_{oc} and fill factor FF from the I-V curve under this irradiance. (iv) Apply these values to the whole device efficiency calculations: $PCE = I_{sc} \cdot V_{oc} \cdot FF / P_{incident}$.

To conclude, the concept of an optical center on a square LSC was proposed based on analytical derivations, where the average optical path of emitted photons from the optical center and the whole device are stipulated to be the same. It is found that the optical center is located at ~82% of the half-length distance from the geometrical center of the planar waveguide. In practice, from the short-circuit current measured at the optical center and the ratio of illumination area, one can predict the short-circuit current of the whole device under uniform illumination. This hypothesis is successfully verified by a $20 \times 20\ \mathrm{cm}^2$ Si QDs-based LSC both for I_{sc} and PCE with a negligible error. This methodology can help access the PV performance of a large-area LSC device by point excitations with basic laboratory instruments.

Funding. Energimyndigheten (46360-2).

Acknowledgment. J.Z. acknowledges funding support from the China Scholarship Council (CSC).

Disclosures. The authors declare no conflicts of interest.

Data availability. Data underlying the results presented in this paper are not publicly available at this time but may be obtained from the authors upon reasonable request.

Supplemental document. See Supplement 1 for supporting content.

REFERENCES

1. I. Fujieda, S. Itaya, M. Ohta, Y. Hirai, and T. Kohmoto, J. Photonics Energy **7**, 028001 (2017).
2. T. Masuda, M. Iyoda, Y. Yasumatsu, S. Dottermusch, I. A. Howard, B. S. Richards, J.-F. Bisson, and M. Endo, Commun. Phys. **3**, 60 (2020).
3. A. Goetzberger and W. Greube, Appl. Phys. **14**, 123 (1977).
4. F. Meinardi, S. Ehrenberg, L. Dhamo, F. Carulli, M. Mauri, F. Bruni, R. Simonutti, U. Kortshagen, and S. Brovelli, Nat. Photonics **11**, 177 (2017).
5. A. Sanguineti, M. Sassi, R. Turrisi, R. Ruffo, G. Vaccaro, F. Meinardi, and L. Beverina, Chem. Commun. **49**, 1618 (2013).
6. T. Wang, J. Zhang, W. Ma, Y. Luo, L. Wang, Z. Hu, W. Wu, X. Wang, G. Zou, and Q. Zhang, Sol. Energy **85**, 2571 (2011).
7. K.-B. Cai, H.-Y. Huang, P.-W. Chen, X.-M. Wen, K. Li, J.-L. Shen, K.-P. Chiu, and C.-T. Yuan, Nanoscale **12**, 10781 (2020).
8. J. Huang, J. Zhou, T. Haraldsson, A. Clemments, M. Fujii, H. Sugimoto, B. Xu, and I. Sychugov, Sol. RRL **4**, 2000195 (2020).
9. S.-J. Ha, J.-H. Kang, D. H. Choi, S. K. Nam, E. Reichmanis, and J. H. Moon, ACS Photonics **5**, 3621 (2018).
10. Y. Li, Y. Sun, and Y. Zhang, Renewable Energy **160**, 127 (2020).
11. Y. Li, Y. Zhang, Y. Sun, and T. Ren, Appl. Opt. **59**, 8964 (2020).
12. I. Sychugov, Appl. Opt. **59**, 5715 (2020).
13. I. Sychugov, Optica **6**, 1046 (2019).
14. J. Huang, J. Zhou, E. Jungstedt, A. Samanta, J. Linnros, L. A. Berglund, and I. Sychugov, ACS Photonics **9**, 2499 (2022).
15. V. Lo Brano, A. Orioli, G. Ciulla, and A. Di Gangi, Sol. Energy Mater. Sol. Cells **94**, 1358 (2010).

Supplemental Document

Optics Letters

Optical center of a luminescent solar concentrator: supplement

JINGJIAN ZHOU,[1,*] JING HUANG,[1,2,3] AND ILYA SYCHUGOV[1,4]

[1]Department of Applied Physics, KTH - Royal Institute of Technology, Stockholm 11419, Sweden
[2]School of Environmental and Biological Engineering, Nanjing University of Science and Technology, Nanjing 210094, China
[3]e-mail: jinghuang@njust.edu.cn
[4]e-mail: ilyas@kth.se
[*]Corresponding author: jingjian@kth.se

Supplement DOI: https://doi.org/10.6084/m9.figshare.20737012

Parent Article DOI: https://doi.org/10.1364/OL.467917

Supporting Information

Optical Center of a Luminescent Solar Concentrator

JINGJIAN ZHOU[1], JING HUANG[1, 2, *], ILYA SYCHUGOV[1, *]

[1]*Department of Applied Physics, KTH - Royal Institute of Technology, Stockholm 11419, Sweden*
[2]*School of Environmental and Biological Engineering, Nanjing University of Science and Technology, Nanjing 210094, China*
**Corresponding author: ilyas@kth.se; jinghuang@njust.edu.cn*

Calculated average optical paths for an isotropic emitter

Optical path lengths from isotropic emitters at different distances from the geometrical center were calculated. Rays were emanating with half-a-degree step. Point positions were chosen both along the orthogonal axes and the diagonal of the square with 0.001*a step. The frequency count of the optical paths was performed and the average value of this distribution was taken for each position. The averaged value between the points on axes and on diagonal directions is presented.

Excitation position-dependent measurements

At each edge, 8 pieces of small-sized Si solar cells (KXOB25, Anysolar, 21 × 6.6 mm^2 active area) are attached, connected in parallel. In each piece of solar cell, 4 p-n junctions are connected in series, capable of delivering ~14 mA short circuit current (I_{sc}) and ~2.7 V open circuit voltage (V_{oc}) under AM1.5G. Note that solar cells are firmly attached to the LSC edges by using pure OSTE as glue and there are no air gaps in between. Our LED-based solar simulator (Sunbrick from G2V optics, ASTM E927 class AAA+, 25 × 25 cm^2) simulates sunlight from 360 nm to 1120 nm with a spectral mismatch of less than 5%.

A set of frontside masks with open windows (1×1 cm^2, distributed from center to the edge, perpendicular to the edge), as shown in the inset of Fig. 2(a), were used to shift the position of point excitations. Only one window was kept open at a time and others were covered by black tapes. The frontside mask can spin on the device to access different directions. Besides, a backside light-absorbing mask was used to minimize the impact from back reflections. Ideally, the light should only enter from the open window. Note that both masks do not directly touch the device (~5 mm in distance), thereby not interrupting the total internal reflection of waveguided light. To eliminate the impact from the possible non-uniformity of simulated sunlight, the open window was always put at the same position under the solar simulator by shifting the device. At the plane of standard AM1.5G, the mobility of this device is limited by the mechanical structure of solar simulator. Instead, 0.9 AM1.5G was applied for the following measurements, which is at ~ 5-6 cm lower plane. To exclude the effect of temperature, all the I_{sc} values were recorded immediately after the exposure to sunlight (it took at least half an hour for the solar simulator to stabilize before measurements).

Optical characterizations of the device

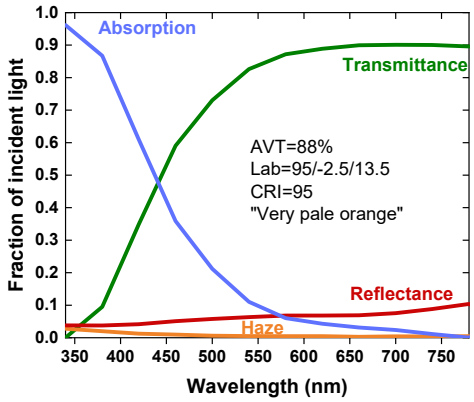

Fig. S1. Transmittance, absorption, reflection and haze spectra of the used LSC.

In the LSC, ~60 mg Si QDs are homogeneously dispersed in the polymer interlayer. According to the color coordinate, the device has a "very pale orange" tint (Colorhexa) [1]. With the emission peak wavelength at 870 nm, a large Stokes shift is present, translating to a negligible reabsorption loss. In addition, the extremely low haze implies a negligible scattering loss.

Estimated absorption fraction of the solar spectrum

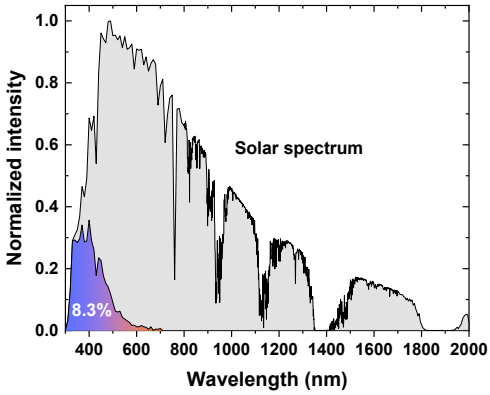

Fig. S2. Absorption fraction under solar spectrum.

According to the measured absorption, this LSC absorbs a fraction of 8.3% sunlight power (absorption above 1000 nm not shown).

Effect of the size of solar cells

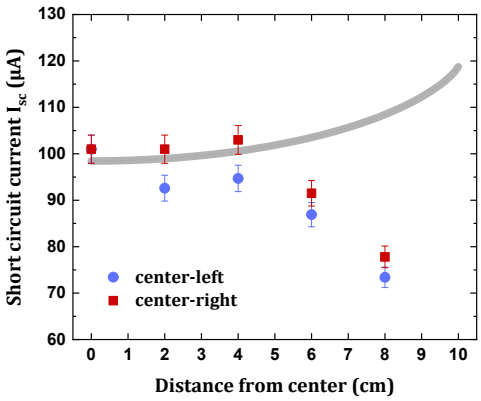

Fig. S3. Short circuit current under point excitations along two directions (center-left in blue and center-right in red) of another 20 × 20 cm^2 LSC attached with longer solar cells. The grey solid line indicates the predicted trend (given an initial I_0 value).

For this LSC (2nd device), 8 pieces of solar cells are connected in parallel to cover its edges. Each solar cell consists of 8 pieces of p-n junctions connected in series. As can be seen, it shows a dropping trend of short circuit current when the illumination window gets close to the edge. This is attributed to the low detection resolution of the large size solar cells, as illustrated in Fig. S4. Due to the fact that in this solar cell 8 pieces of p-n junctions are connected in series, the short circuit current will be limited by the lowest I_{sc} among p-n junctions, which corresponds to the longest optical path from the excitation point (red lines in Fig S4, left). This limitation becomes dominant when the illumination window is close to the edge (left). While for a small size of solar cell (right), this effect has a low impact.

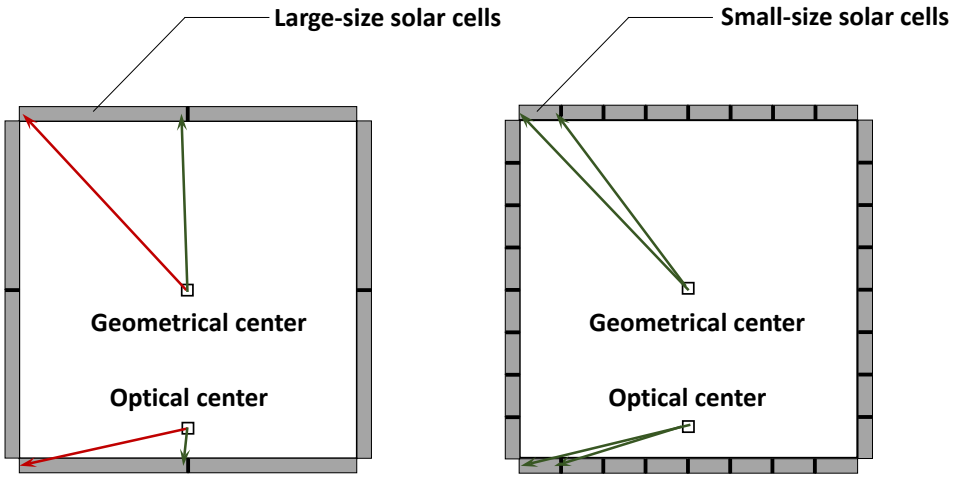

Fig. S4. Schematics of the resolution provided by different solar cell coupling at the edges: (left) 2nd device with long solar cells, and (right) the main device reported in this work with short solar cells connected in parallel. Irradiance within one solar cell is relatively uniform, which is nearly independent on the excitation spot position (green lines).

Estimation of the open circuit voltage and fill factor

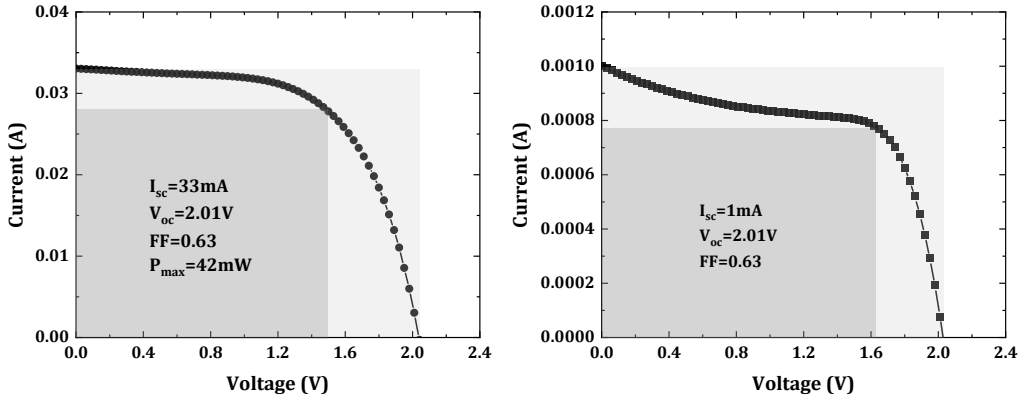

Fig. S5. I-V characteristic curves of the LSC under uniform illumination (left) and single solar cell delivering ~1 mA short circuit current (right).

By mimicking the irradiance on a single solar cell, almost the same open circuit voltage and fill factor can be obtained.

Another method estimating V_{oc} and FF

The relationship between the open circuit voltage (V_{oc}) of silicon solar cells and the incident irradiance (E) can be easily calibrated by a set of data measured under the solar simulator based on a well-known dependence $V_{oc} = V_0 - a\ln(E_0 / E)$ [2]. For the solar cells used here, V_0=2.5 V, E_0=1000 W/m^2, a=0.203. Then, extracting irradiance level from the measured LSC solar cell short circuit current, one can predict the open circuit voltage. As a reference, the I_{sc} of single piece of solar cell under one sun (1000 W/m^2 in irradiance) was measured to be 13 mA. With 32 mA total I_{sc} of the LSC-attached solar cells one can estimate on average that each piece of solar cells here contributes to ~1 mA (32 pieces in parallel). Since the short circuit current increase with the incident irradiance linearly, the irradiance on a single LSC-attached solar cell can be estimated as 77 W/m^2. Thus, the estimated V_{oc} from equation above is ~1.98 V (~2% error to the measured one 2.01 V). Finally, from the specifications of solar cells, an average fill factor (~0.65) can be used for the estimation of PCE.

Reference

1. C. Yang, D. Liu, and R. R. Lunt, Joule **3**, 2871-2876 (2019).
2. V. Lo Brano, A. Orioli, G. Ciulla, and A. Di Gangi, Sol. Energy Mater. Sol. Cells **94**, 1358-1370 (2010).